

## SPECKLE OBSERVATIONS AND ORBITS OF MULTIPLE STARS

ANDREI TOKOVININ

Cerro Tololo Inter-American Observatory, Casilla 603, La Serena, Chile

MARK E. EVERETT

National Optical Astronomy Observatory, 950 North Cherry Avenue, Tucson, AZ 85719, USA

ELLIOTT P. HORCH\*

Department of Physics, Southern Connecticut State University, 501 Crescent Street, New Haven, CT 06515, USA

GUILLERMO TORRES

Center for Astrophysics — Harvard & Smithsonian, 60 Garden Street, Cambridge, MA 02138, USA

DAVID W. LATHAM

Center for Astrophysics — Harvard & Smithsonian, 60 Garden Street, Cambridge, MA 02138, USA

*Draft version September 2, 2019*

### ABSTRACT

We report results of speckle-interferometric monitoring of visual hierarchical systems using the newly commissioned instrument NESSI at the 3.5-m WIYN telescope. During one year, 390 measurements of 129 resolved subsystems were made, while some targets were unresolved. Using our astrometry and archival data, we computed 36 orbits (27 for the first time). Spectro-interferometric orbits of seven pairs are determined by combining positional measurements with radial velocities measured, mostly, with the Center for Astrophysics digital speedometers. For the hierarchical systems HIP 65026 (periods 49 and 1.23 years) and HIP 85209 (periods 34 and 1.23 years) we determined both the inner and the outer orbits using astrometry and radial velocities and measured the mutual orbit inclinations of  $11^{\circ}3 \pm 1^{\circ}0$  and  $12^{\circ}0 \pm 3^{\circ}0$ , respectively. Four bright stars are resolved for the first time; two of those are triple systems. Several visual subsystems announced in the literature are shown to be spurious. We note that subsystems in compact hierarchies with outer separations less than 100 au tend to have less eccentric orbits compared to wider hierarchies.

*Keywords:* binaries:visual

### 1. INTRODUCTION

We know that the majority of multi-planet systems are co-planar (Fabrycky et al. 2014), as well the planets found around eclipsing binaries (e.g. Kepler-1647, Kostov et al. 2016). Low-mass triple systems with outer separations of the order of  $\sim 50$  au or less also have a strong alignment trend, even though the typical relative angles between orbital planes are still substantial,  $\sim 30^{\circ}$  (Tokovinin 2017). Formation of companions in a massive circumstellar disc, their subsequent growth and inward migration seem to match the prevalent architecture of compact “planetary-like” (i.e. quasi-coplanar) triple systems. One of the natural outcomes of this scenario are close (eclipsing) binaries surrounded by a remnant disk, from which the circumbinary planets condense, as demonstrated by the *Kepler* discovery of such systems. Recent modeling by Moe & Kratter (2018) shows that migration in a disc is also necessary for explaining the observed fraction of solar-type close binaries, while the

alternative channel of close-binary formation via dynamical evolution of misaligned triple systems, also relevant for formation of hot Jupiters (Fabrycky & Tremaine 2007), is not efficient enough.

The distribution of relative inclinations in triple systems is an essential input to those studies. Orbits of binary and triple systems contain a fossil record of the conditions prevailing during their formation. While migration in a disk produces quasi-coplanar systems, misaligned systems diagnose alternative formation mechanisms. For example, frequent dynamical interactions between stars in dense clusters or accretion of misaligned gas produce multiple systems with misaligned orbits, binaries with misaligned stellar spins and, later, planetary systems that are not confined to one plane.

Although stellar triples have been known for a long time, advances in the observational techniques have only recently given access to the most interesting close and fast systems with spatial scales of  $\sim 10$  au, matching the typical size of discs and planetary systems. For some of those, it has been possible to determine both inner and outer orbits and their relative orientation (Tokovinin et al. 2015; Tokovinin & Latham 2017). However, much work remains to be done. Ongoing high-

Electronic address: atokovinin@ctio.noao.edu

Electronic address: everett@noao.edu

\*Adjunct Astronomer, Lowell Observatory

Electronic address: horche2@southernct.edu

Electronic address: gtorres@cfa.harvard.edu

Electronic address: dlatham@cfa.harvard.edu

resolution surveys, particularly in the solar neighborhood, continue to discover compact hierarchical systems (Horch et al. 2019). Follow-up astrometric monitoring on a time scale from years to decades is needed to map the orbital motion and to define the architecture of those systems. These data, in turn, will provide insights on the formation history of stars and planets.

The highly efficient speckle program at the Southern Astrophysical Research Telescope (SOAR) assigns top priority to the study of orbital motions in resolved triple systems (see Tokovinin et al. 2018, and references therein). As a result, tens of triples already have new or updated accurate orbits while monitoring of other systems continues. We are extending this effort to the northern sky using the recently commissioned NESSI instrument on the 3.5-m WIYN telescope (Scott et al. 2018).

Our targets were selected from the current version of the Multiple-Star Catalog (Tokovinin 2018b). We observed resolved northern subsystems with unknown orbits and estimated orbital periods shorter than 100 yr. This speckle program at WIYN pursues three main goals.

- Determination or improvement of visual orbits for members of hierarchical systems, especially those with short periods. Orbits contribute to the statistics of periods, relative inclinations, and eccentricities.
- Positional measurements and relative photometry of subsystems with periods of a few decades for future orbit determinations.
- Verification of uncertain subsystems. Identification of spurious triple stars cleans the statistics and saves efforts for their future monitoring.

In this paper we report speckle observations at the WIYN telescope conducted during one year, from 2018 February to 2019 January. The instrument, observing procedure, and data reduction are covered in Section 2. The results (new measurements and orbits) are presented in Section 3. Section 4 summarizes our work.

## 2. OBSERVATIONS

### 2.1. The instrument

The speckle camera at the WIYN telescope is called NESSI for *NASA-NSF Exoplanet Observational Research (NN-EXPLORE) Exoplanet Stellar Speckle Imager*. This is a dual-channel imaging instrument (Scott et al. 2018). The beam arriving from the telescope is collimated, divided into two color channels by a dichroic beamsplitter, and re-focused on two identical electron-multiplication CCD cameras with a magnification of  $1.5\times$  or a pixel scale of 18.2 mas. Wavelengths longer than 673 nm pass through the dichroic to the red channel, while shorter wavelengths are reflected to the blue channel. Both channels have additional filters. Here we used the 562.3/43.6 nm filter in the blue channel and the 716.0/51.5 nm in the red channel (some observations were obtained instead in the 832.0/40.4 nm filter). NESSI does not have an atmospheric dispersion corrector. The position angle on the sky is maintained by the WIYN instrument rotator. In the blue channel, the image is oriented with North pointing to the left and East pointing down. In the red channel, the horizontal orientation is inverse (North pointing

right). Further information on NESSI is provided by Scott et al. (2018).

### 2.2. Observing procedure

On each target, we registered sub-frames of  $256\times 256$  pixels ( $4''.8$  on the sky) with a short exposure of 40 ms. The electron multiplication gain was adjusted depending on the star brightness. A sequence of 1000 such frames (the data cube) is recorded in the FITS file. Auxiliary information (target name, coordinates, filters, and time of observation) is kept in the text files of observing logs, one per night. We recorded from 2 to 8 sequential data cubes of the object and one data cube of the reference star, selected from the Bright Star Catalog in the vicinity of the target. The bright star is used as a reference in the data processing.

Forty hours of service observations were allocated to this program by the NASA-WIYN TAC (programs 18A-0122 and 18B-0008). Our objects, reference stars, and calibration binaries were observed together with other programs. The data used in this paper have been obtained during 33 nights in the period from 2018 February 2 to 2019 January 30. A total of 2057 data cubes were recorded, amounting to 23 hours of the open-shutter time.

### 2.3. Data processing and calibration

All NESSI data cubes are normally processed using the speckle image reconstruction pipeline (Scott et al. 2018). However, for multiple stars the image reconstruction is not strictly necessary (images from the NESSI pipeline are used here for illustration). We adapted the SOAR speckle pipeline (see Tokovinin, Mason, & Hartkopf 2010; Tokovinin 2018a) written in IDL. The most computer-intensive part of the pipeline is the calculation of the power spectra. After reading the image cube into the memory, the code first determines the centroids in each frame, thresholded at 10 counts above the background (the threshold is less than one electron and therefore does not distort the linearity). Frames where the star is too close to the edge are rejected. Then the power spectrum is accumulated, as well as re-centered images and the shift-and-add (SAA) images centered on the brightest pixel in each frame. The orientation of images in the red channel is changed to match the blue channel.

Further data processing uses only the two-dimensional images and power spectra. It is organized by means of the data structure that keeps all relevant parameters and the processing results for each data cube and each channel, i.e. from 4 to 16 records for a given target and, typically, two records for the reference star. The essential information is ingested from the text files of the observing logs and complemented by calculation of additional parameters such as the zenith distance and parallactic angle. Results of the data analysis (e.g. the signal level in the power spectrum, estimates of the resolution and detection limits, and binary-star parameters) are also kept in this structure. Final results are obtained by averaging similar data on a given target, separately for the blue and red channels. A more detailed description of the SOAR speckle pipeline can be found in Tokovinin (2018a).

Parameters of binary stars (separation  $\rho$ , position angle  $\theta$ , and magnitude difference  $\Delta m$ ) are determined

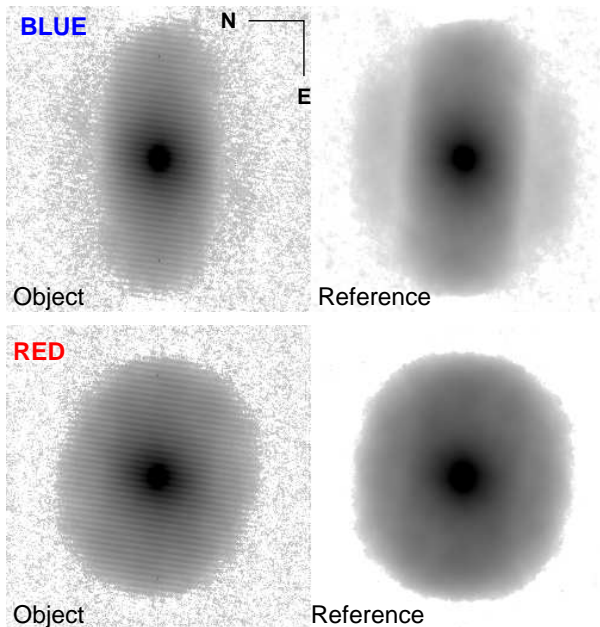


**Figure 1.** Example of the power spectra in the blue (top) and red (bottom) channels of NESSI. The object (on the left) is a  $0''.91$  binary BU 403 (WDS J04257–0214), evidenced by the finely spaced horizontal fringes. Power spectra of the reference star are shown on the right. The zero spatial frequency is at the center of each frame, the power spectra are rendered in negative logarithmic scale. The atmospheric dispersion of 4.6 and 1.3 pixels in the blue and red channels, respectively (zenith distance  $34^\circ 2'$ ) reduces the resolution in the North-South direction.

by modeling the observed power spectrum as a product of the reference spectrum and the binary-star fringes (Tokovinin, Mason, & Hartkopf 2010). Uncorrected atmospheric dispersion damps the power spectrum in the vertical direction, as illustrated in Figure 1. The NESSI filters have a rectangular bandpass, hence the damping factor has a shape of the  $\text{sinc}^2(x)$  function with sidelobes. The loss of resolution is particularly important in the blue channel, offsetting the greater resolving power at shorter wavelengths. As the object and reference are observed close to each other, the model adequately accounts for the dispersion. Triple stars are fitted similarly.

We compared the relative scale and orientation in the blue and red channels using 24 binaries with separations larger than  $0''.5$  and  $\Delta m < 3$  mag. The red camera has been removed between some runs, and, as a result, the total range of relative angular offsets between the channels is  $1^\circ 2'$ . On the other hand, the difference in the scale factor is quite consistent: pixels in the red camera are larger by 0.8%. We corrected the astrometry in the red channel for scale and angle offsets to match the blue channel.

Twelve relatively wide binaries observed at WIYN in 2018 February and June belong to the list of SOAR calibrators with accurately modeled motion (Tokovinin 2018a). The mean angular offset of WIYN measurements of those stars relative to their models is  $-0''.15$  with an rms scatter of  $0''.17$ ; their separations match the model to within 0.3%. We corrected for the angular offset and left the separations as measured, thus confirming the nominal pixel scale of the NESSI blue channel, 18.2 mas. We assume here that the calibration of angle and pixel scale of NESSI remained stable throughout the whole year.

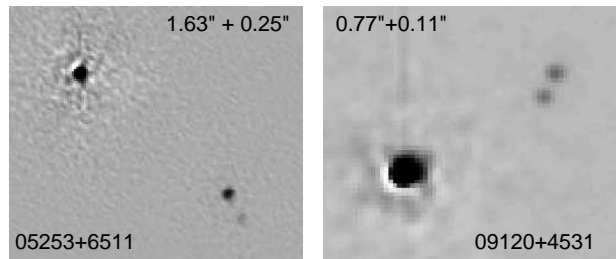


**Figure 2.** Reconstructed images of two triple systems in the red channel. Left: WDS J05253+6511 (HDS 711 A,Ba and BAG 17 Ba,Bb) observed in 2018.1. Right: WDS J09120+4531 (YSC 91 A,Ba and Ba,Bb) observed in 2019.1. Separations of the wide and close pairs are indicated.

A more detailed study of the calibration would require repeated measurements of a larger number of wide calibration pairs, not available in this data set. We note that residuals of our measurements to good-quality orbits are small, confirming independently the absence of systematic errors at the level of  $<0''.5$  in angle and  $<0.5\%$  in scale.

#### 2.4. Radial velocities

Radial velocities for several systems have been obtained at the Harvard-Smithsonian Center for Astrophysics (CfA) using several instruments on different telescopes. The Digital Speedometers (see Latham 1992) were used on 1.5 m telescopes at the Oak Ridge Observatory (Harvard, Massachusetts) and the Fred L. Whipple Observatory (Mount Hopkins, Arizona), and on the Multiple Mirror Telescope with equivalent aperture of 4.5 m (also on Mount Hopkins) before its conversion to a monolithic 6.5 m telescope. In these instruments, intensified photon-counting Reticon detectors delivered a single echelle order  $45 \text{ \AA}$  wide centered at  $5187 \text{ \AA}$  (featuring the Mg I b triplet) at a resolving power of 35,000.

We also used the Tillinghast Reflector Echelle Spectrograph (TRES; Szentgyorgyi & Fűrész 2007; Fűrész 2008) attached to the 1.5 m telescope on Mount Hopkins, which covers the wavelength range  $3900\text{--}9100 \text{ \AA}$  in 51 orders at a resolving power of 44,000. Most data come from the CfA spectrometers, while TRES contributed 34 observations, mostly of HIP 85209.

Radial velocities were measured by cross-correlation using suitable synthetic or observed templates centered on the Mg I b triplet. For systems showing double or triple lines we used the two-dimensional or three-dimensional correlation techniques TODCOR (Zucker & Mazeh 1994) and TRICOR (Zucker et al. 1995), with a separate template for each stellar component. The RVs are given below in Table 5 together with their residuals from the orbits. The CfA RVs are given on the native instrument system (a correction of  $+0.14 \text{ km s}^{-1}$  would be needed to bring them to the IAU system). The RVs measured with TRES have been corrected to the same zero point as the velocities from the CfA Digital Speedometers, so they also need to be corrected by  $+0.14 \text{ km s}^{-1}$  to put them on the IAU system.

### 3. RESULTS

#### 3.1. Speckle measurements

The results (measurements of resolved pairs and non-resolutions) are presented in almost the same format as

**Table 1**  
Measurements of multiple stars at WIYN

Col.	Label	Format	Description, units
1	WDS	A10	WDS code (J2000)
2	Disc.	A16	Discoverer code
3	Other	A12	Alternative name
4	RA	F8.4	R.A. J2000 (deg)
5	Dec	F8.4	Declination J2000 (deg)
6	Epoch	F9.4	Julian year (yr)
7	Filt.	A3	Filter ( $\lambda$ in nm)
8	$N$	I2	Number of averaged cubes
9	$\theta$	F8.1	Position angle (deg)
10	$\rho\sigma_\theta$	F5.1	Tangential error (mas)
11	$\rho$	F8.4	Separation (arcsec)
12	$\sigma_\rho$	F5.1	Radial error (mas)
13	$\Delta m$	F7.1	Magnitude difference (mag)
14	Flag	A1	Flag of magnitude difference <sup>a</sup>
15	(O-C) $_\theta$	F8.1	Residual in angle (deg)
16	(O-C) $_\rho$	F8.3	Residual in separation (arcsec)
17	Ref.	A8	Orbit reference <sup>b</sup>

<sup>a</sup> Flags: q – the quadrant is determined; \* –  $\Delta m$  and quadrant from average image; : – noisy data.

<sup>b</sup> References to VB6 are provided at <http://ad.usno.navy.mil/wds/orb6/wdsref.txt>

in the papers reporting observations at SOAR. The long tables are published electronically; here we describe their content. Figure 2 shows .images of two triple systems reconstructed by the NESSI pipeline. Although the measurements are obtained from the power spectra, the reconstructed images of selected triple systems illustrate the imaging capability of NESSI.

Table 1 lists 390 measurements of 129 resolved pairs and subsystems, including new discoveries. The pairs are identified by their Washington Double Star (WDS) codes and discoverer designations adopted in the WDS catalog (Mason et al. 2001), as well as by alternative names in column (3), mostly from the *Hipparcos* catalog. Equatorial coordinates for the equinox and epoch J2000 in degrees are given in columns (4) and (5) to facilitate matching with other catalogs and databases. Column (6) lists the dates of observation in Julian years, column (7) the filters, column (8) the numbers of averaged measurements from individual data cubes. The measurements (position angles  $\theta$ , errors in the tangential direction  $\rho\sigma_\theta$ , separations  $\rho$ , radial errors  $\sigma_\rho$ , and magnitude differences  $\Delta m$ ) are given in columns (9) to (13), respectively. In the case of multiple systems, the position measurements and their errors and magnitude differences refer to the individual pairings between components, not to their photocenters.

We list the internal errors derived from the power spectrum model and from the difference between the measurements in several data cubes (Tokovinin, Mason, & Hartkopf 2010) and do not include systematic errors. The median error is 0.4 mas, and 94% of errors are less than 4 mas. The real errors are somewhat larger, especially for difficult pairs with substantial  $\Delta m$  and/or with small separations (an example of such challenging pair 12576+3514 Aa,Ab is given below in Section 3.3). We checked the estimated internal errors by comparing the measurements in the blue and red channels and computing  $\chi_\rho^2 = (\rho_b - \rho_r)^2 / (\sigma_{\rho,b}^2 + \sigma_{\rho,r}^2)$  and an analogous  $\chi_\theta^2$  using 114 pairs measured in both channels simultaneously. The median  $\chi^2$  values are 2.1

**Table 2**  
Unresolved stars

Col.	Label	Format	Description, units
1	WDS	A10	WDS code (J2000)
2	Disc.	A16	Discoverer code
3	Other	A12	Alternative name
4	RA	F8.4	R.A. J2000 (deg)
5	Dec	F8.4	Declination J2000 (deg)
6	Epoch	F9.4	Julian year (yr)
7	Filt.	A3	Filter
8	$N$	I2	Number of averaged cubes
9	$\rho_{\min}$	F7.3	Angular resolution (arcsec)
10	$\Delta m(0.15)$	F7.2	Max. $\Delta m$ at 0''.15 (mag)
11	$\Delta m(1)$	F7.2	Max. $\Delta m$ at 1'' (mag)

and 1.6 in  $\rho$  and  $\theta$ , respectively, with a large scatter;  $\chi^2$  do not correlate with  $\rho$  and  $\Delta m$ . The scatter is reduced and the  $\chi^2$  medians approach the expected value of one if the instrumental errors of 0.3 and 0.15 mas in the radial and tangential directions are added quadratically. These numbers quantify the typical difference between the internal and external errors of our astrometry.

The flags in column (14) indicate cases when the true quadrant is determined from the SAA images (otherwise the position angle is measured modulo 180°), when the photometry of wide pairs is derived from the long-exposure images (this reduces the bias caused by speckle anisoplanatism) and when the data are noisy or the resolutions are tentative. For binary stars with known orbits, the residuals to the latest orbit and its reference are provided in columns (15)–(17). The orbits computed or updated here are denoted as WIYN2019.

Non-resolutions (including those of reference stars) are reported in Table 2. Its first columns (1) to (8) have the same meaning and format as in Table 1. Column (9) gives the minimum resolvable separation when pairs with  $\Delta m < 1$  mag are detectable. It is computed from the maximum spatial frequency of the useful signal in the power spectrum and is normally close to the formal diffraction limit  $\lambda/D$ . The following columns (10) and (11) provide the indicative dynamic range, i.e. the maximum magnitude difference at separations of 0''.15 and 1'', respectively.

### 3.2. New and updated visual orbits

Our measurements together with previous observations allow the calculation of orbits for several subsystems. We consulted the WDS catalog and the recent literature for the existing data. However, for many pairs with long periods the available data do not constrain their orbital elements, allowing a wide range of potential solutions. We provide here preliminary (grade 5) orbits of such pairs. Although these crude orbits are not suitable for measurements of stellar masses or relative orbit orientation in triple systems, their publication still makes sense for improving the statistics (even an uncertain orbit is better than no orbit) and planning future observations. To illustrate this situation, two preliminary orbits are shown in Figure 3. Good coverage of these systems with periods of  $\sim 200$  years will be reached only after several more decades of monitoring. Meanwhile, their preliminary orbits adequately describe the observed motion and will not need an update in the near term.

The elements of visual orbits determined here are listed

**Table 3**  
Visual orbits

WDS	Disc.	$P$ (yr)	$T$ (yr)	$e$	$a$ (arcsec)	$\Omega_{2000}$ (deg)	$\omega$ (deg)	$i$ (deg)	Grade	Reference <sup>a</sup>
01500+7456	MLR 297 AB,C	197.5	1961.5	0.0	0.429	128.1	0.0	72.3	5	new
02529+5300	A 2906 A,B	89.6	1972.88	0.93	0.181	17.9	85.6	135.4	4	new
		$\pm 4.5$	$\pm 0.79$	fixed	$\pm 0.012$	$\pm 15.8$	$\pm 10.2$	$\pm 4.8$		
03127+7133	STT 50 A,B	583	2418.5	0.428	1.866	31.0	112.2	113.9	4	Sca2012b
		$\pm 15$	$\pm 15$	$\pm 0.023$	$\pm 0.065$	$\pm 0.9$	$\pm 1.7$	$\pm 0.9$		
04192+6135	BU 1333 B,C	180.0	2043.6	0.67	0.238	49.3	150.0	126.9	5	new
04480+5645	HDS 617 Aa,Ab	90	2027.8	0.87	0.503	54.5	235.9	120.0	5	new
05237+7347	A 843 A,B	181.9	2036.3	0.80	0.556	27.0	230.0	86.8	4	new
		$\pm 11.6$	$\pm 1.3$	fixed	$\pm 0.023$	$\pm 1.5$	fixed	$\pm 0.4$		
07211+6740	JNN 55 B,C	13.97	2013.53	0.78	0.178	94.5	106.7	67.9	4	new
		$\pm 1.23$	$\pm 0.90$	fixed	$\pm 0.040$	$\pm 6.5$	$\pm 7.4$	$\pm 7.8$		
07295+3556	JNN 57 Aa,Ab	18.4	2016.84	0.568	0.158	244.1	132.9	113.3	3	new
		$\pm 2.9$	$\pm 0.66$	$\pm 0.134$	$\pm 0.028$	$\pm 9.6$	$\pm 12.4$	$\pm 8.4$		
08307+4645	YSC 3 Aa,Ab	19.32	2002.35	0.0	0.095	112.5	0.0	71.5	4	new
		$\pm 0.34$	$\pm 0.18$	fixed	$\pm 0.004$	$\pm 1.7$	fixed	$\pm 1.9$		
09186+2944	A 221 Ba,Bb	184	1888.1	0.90	0.591	142.3	82.7	99.2	5	new
09354+3958	COU 2084 Aa,Ab	50.34	2012.39	0.652	0.246	84.7	137.0	112.8	3	new
		$\pm 1.91$	$\pm 0.82$	$\pm 0.036$	$\pm 0.012$	$\pm 1.7$	$\pm 6.9$	$\pm 3.4$		
10454+3831	HO 532 A,C	326	1883	0.90	3.482	154.0	95.3	96.0	5	Mnt2000a
11017+3641	HDS 1574 Aa,Ab	46.22	2013.14	0.795	0.235	169.6	337.5	116.4	4	new
		$\pm 2.57$	$\pm 0.98$	$\pm 0.030$	$\pm 0.011$	$\pm 5.8$	$\pm 14.3$	$\pm 3.2$		
11017+3641	COU 1422 Ba,Bb	173	1958.0	0.35	0.56	74	180	39.5	5	new
11151+3735	CHR 192 Aa,Ab	200	2019.3	0.486	0.2224	254.2	11.2	111.7	5	new
12089+2147	HDS 1714 Aa,Ab	235.6	2029.2	0.80	0.5979	41.1	219.9	80.3	5	new
14353+4302	LSC 56 Aa,Ab	11.23	2009.85	0.30	0.0473	112.9	90.0	77.1	4	new
		$\pm 1.92$	$\pm 0.88$	$\pm 0.26$	$\pm 0.0057$	$\pm 3.3$	fixed	$\pm 6.0$		
16147+3352	YSC 152 Ea,Eb	52.0	1994.267	0.0	0.514	214.9	0.0	60.5	5	Hei1990d
19514+4044	COU 2530 A,B	55.0	2022.9	0.40	0.250	159.6	38.4	74.2	4	new
		$\pm 4.8$	$\pm 1.0$	fixed	$\pm 0.007$	$\pm 1.5$	$\pm 8.6$	$\pm 1.3$		
20599+4016	HDS 2989 Da,Db	212.7	2142.3	0.85	0.940	154.5	270.0	90.9	5	new
21308+4827	A 770 A,B	146	1958.6	0.20	0.307	321.4	90.0	89.5	5	new
22139+3943	MCA 70 Aa,Ac	125.0	2028.8	0.82	0.324	166.1	26.0	54.6	5	new
22359+3938	CHR 112 Aa,Ab	41.6	2022.9	0.44	0.057	119.7	107.9	69.1	3	new
		$\pm 5.4$	$\pm 2.4$	$\pm 0.19$	$\pm 0.007$	$\pm 5.2$	$\pm 5.6$	$\pm 6.4$		

<sup>a</sup> References: Hei1990d – Heintz (1990); Lin2012b – Ling (2012); Mnt2000a – Mante (2000); Sca2012b – Scardia et al. (2012)

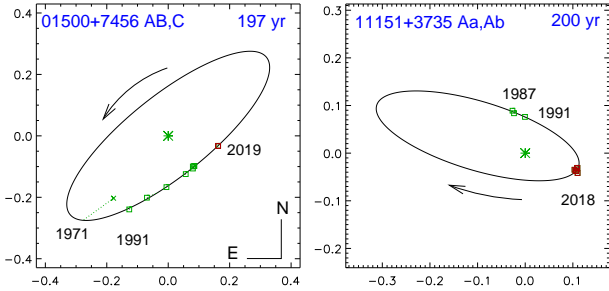


**Figure 3.** Preliminary (grade 5) orbits of two long-period subsystems. In these and following plots, the primary component is placed at the coordinate origin. The axis scale is in arcseconds, North is directed up and East to the left. Squares denote the measurements (less accurate measurements are plotted as crosses); short dotted lines connect them to the corresponding positions on the orbit (ellipse). Dates of some measurements are indicated, the measurements at WIYN are plotted in red.

in Table 3 in standard notation. The position angles were corrected for precession, so the nodes  $\Omega$  refer to the J2000 epoch. The orbits were computed by least-squares fitting with weights inversely proportional to the adopted measurement errors; the IDL code ORBIT (Tokovinin 2016) was used. The two ultimate columns give the provisional grade and the reference to previously published orbits, when available. We do not list formal errors for preliminary orbits of grade 5. Orbits of grades 4 and 3 are plotted in Figure 4.

Individual positional measurements and their residuals

from the orbits are listed in Table 4, published in full electronically. Similarly, the RVs used in combined orbits and their residuals are listed in Table 5. These tables also contain measurements and residuals for combined orbits presented in Section 3.3 and for the hierarchies covered in Sections 3.4, 3.5, and 3.6.

Below we comment on some of those systems. The information is taken from the MSC (Tokovinin 2018b) and the *Gaia* DR2 (Gaia collaboration 2018). Comparison of the *Gaia* short-term proper motion (PM) with the long-term PM computed from the *Gaia* and *Hipparcos* positions allows in some cases to detect the PM difference  $\Delta\mu$  (astrometric acceleration), see Brandt (2018). It should be directed oppositely to the motion of the secondary component predicted by our orbits. We denote here subsystems by joining components’ designations with a comma (e.g. A,B). In a triple system with a tertiary component C, AB without comma means the center of gravity of the inner pair A,B and AB,C refers to the outer orbit.

01500+7456 MLR 297 AB,C (HIP 8533) moves slowly on a 200 yr orbit (Figure 3). The 0<sup>h</sup>06 subsystem BAG 16 A,B with a much shorter expected period of  $\sim 15$  yr was resolved in 2018.08 but closed down in 2018.9 (we use only the latter measurement for the outer orbit). The *Gaia* parallax of  $7.4 \pm 0.7$  mas has a large error that might be caused by the subsystem A,B. However, some measurements attributed in the WDS to this inner pair actually refer to AB,C and fit its orbit.

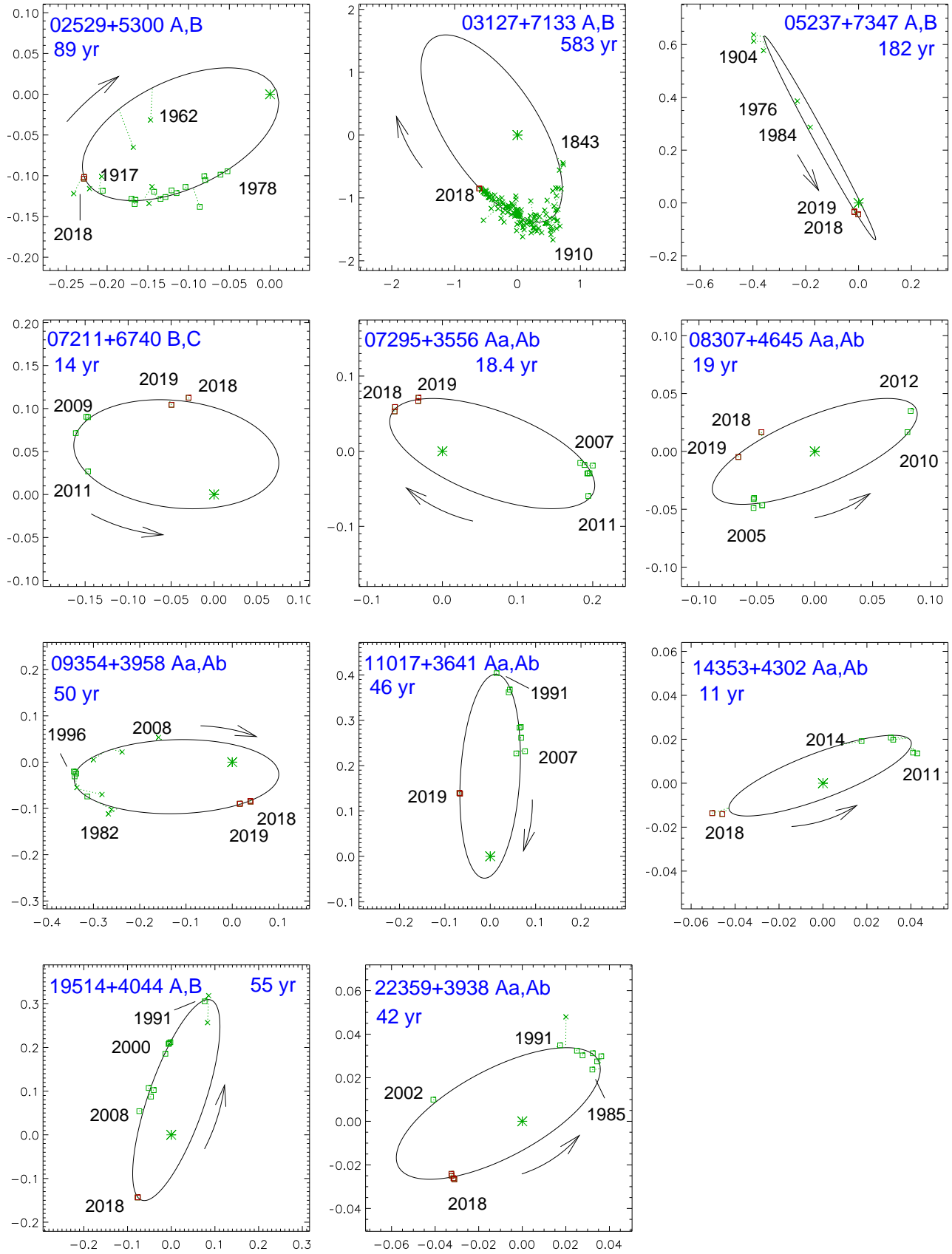


**Figure 4.** Visual orbits of grades 3 and 4 (see the legend to Figure 3).

**Table 4**  
Position measurements and residuals (fragment)

WDS	Disc.	Date (yr)	$\theta$ ( $^{\circ}$ )	$\rho$ ( $''$ )	$\sigma_{\rho}$ ( $''$ )	$(O-C)_{\theta}$ ( $^{\circ}$ )	$(O-C)_{\rho}$ ( $''$ )	Ref. <sup>a</sup>
00541+6626	YSC 19 Aa,Ab	2018.6496	134.6	0.0800	0.0050	0.0	-0.0024	W
00541+6626	YSC 19 Aa,Ab	2018.6496	134.0	0.0820	0.0050	-0.6	-0.0004	W
01500+7456	MLR 297 AB,C	1971.5900	138.5	0.2700	0.1500	5.0	-0.1395	M
01500+7456	MLR 297 AB,C	1991.2500	152.0	0.2710	0.0100	1.2	-0.0014	H
01500+7456	MLR 297 AB,C	1999.8115	161.0	0.2129	0.0050	-6.7	0.0208	s
01500+7456	MLR 297 AB,C	2000.8743	178.0	0.1670	0.0050	7.2	-0.0157	s
01500+7456	MLR 297 AB,C	2007.8215	204.7	0.1370	0.0050	4.3	0.0006	s
01500+7456	MLR 297 AB,C	2010.7130	217.2	0.1334	0.0050	-0.0	0.0029	s

<sup>a</sup> H: Hipparcos; h: HST; M: visual micrometer measures; s: speckle interferometry or lucky imaging at other telescopes; a: adaptive optics; G: Gaia; W: speckle interferometry at WIYN.

**Table 5**  
Radial velocities and residuals (fragment)

WDS	Disc.	Date (HJD -2400000)	RV	$\sigma$ (km s $^{-1}$ )	(O-C)	Comp. Instr. <sup>a</sup>
00541+6626	YSC 19 Aa,Ab	52958.7366	-11.99	0.85	-0.12	a
00541+6626	YSC 19 Aa,Ab	52984.6649	-11.36	0.85	0.08	a
00541+6626	YSC 19 Aa,Ab	53013.6392	-10.85	0.86	0.12	a
02249+3039	HDS 314 Aa,Ab	49198.8524	1.62	0.47	0.61	a
02249+3039	HDS 314 Aa,Ab	49237.8599	0.18	0.42	-0.85	a
02249+3039	HDS 314 Aa,Ab	49261.6807	1.49	0.43	0.45	a

<sup>a</sup> Components: a – primary, b – secondary, c – tertiary. RVs from the CfA digital speedometers have no instrument codes. Otherwise, RVs measured from the TRES spectra are marked by T, RVs from Sperauskas et al. (2019) by S, RVs from Tokovinin & Smekhov (2002) by t, and RVs from *Gaia* DR2 by G.

02529+5300 A 2906 A,B (HIP 13424, HR 846) has passed through the periastron of its eccentric ( $e = 0.9$ ) 90 yr orbit in 1973 and presently is again near the apastron, close to the position where it has been discovered a century ago by R. Aitken. The measurements cover one full revolution and constrain the orbit reasonably well (grade 4). The tertiary component C at  $1''.57$  has been known since 1825. Although *Gaia* gives for C slightly discrepant parallax and PM, the outer pair is likely physical, considering the low chance of finding such a bright ( $V_C = 7.25$  mag) star so close to AB. The estimated period of AB,C is  $\sim 2$  kyr and its observed slow motion does not contradict this estimate.

03127+7133 STT 50 A,B (HIP 14944). The orbit of Scardia et al. (2012) is corrected here from  $P = 309$  yr to  $P = 583$  yr and assigned grade 4. The subsystem Sca 171 Aa,Ab is not confirmed, so this appears to be a binary.

04192+6135 BU 1333 B,C. The measurements cover one century and the orbital period is about 180 yr. The pair is closing and will pass through the periastron in 2044. The main component A (HIP 20157) remains at  $5''.3$  separation from BC since the discovery of A,B by W. Struve in 1830; the period of A,BC is  $\sim 15$  kyr.

04480+5645 HDS 617 Aa,Ab is the bright star 4 Cam (HR 1511, HIP 22287) resolved by *Hipparcos* at  $0''.6$ . Now it closed to  $0''.23$  and approaches the periastron of its preliminary eccentric ( $e = 0.87$ ) 90 yr orbit, predicted for 2027. The faint ( $V = 13.2$  mag) physical tertiary component B is located at  $13''.8$  from A.

05237+7347 A 843 A,B (HD 34254) was discovered in 1904 by R. Aitken at  $0''.7$  and presently has closed down to  $0''.04$ . Its first orbit with  $P = 182$  yr is not sufficiently constrained by available observations. It is fitted with a fixed eccentricity of  $e = 0.80$  and fixed  $\omega$ , chosen to yield a reasonable mass sum. The physical tertiary component C is located at  $80''$  from AB.

07211+6740 JNN 55 B,C is a nearby (26 pc) pair of M3V and M5V dwarfs discovered in 2008 (Janson et al. 2012). Its first orbit with  $P = 14$  yr is computed from measurements at five epochs. The period and eccentricity are fixed to match the expected mass sum of  $0.5 M_\odot$ . Further monitoring for a few more years will constrain all elements. The K0V primary component A (HIP 35628) is located at  $20''.7$  from BC.

07295+3556 JNN 57 Aa,Ab is a young pair of M1V dwarfs at 42 pc belonging to the  $\beta$  Pictoris moving group (Alonso-Floriano et al. 2015). Its first orbit with  $P = 18.4$  yr is sufficiently well constrained by nine measurements taken during 11 years. The tertiary component B is located at  $95''.5$ .

08307+4645 YSC 3 Aa,Ab (HIP 41739, distance 118 pc). Owing to the small  $\Delta m$ , the quadrants are not certain; they were changed in two instances to match our circular, still preliminary orbit. The tertiary component B at  $1''.2$  is also measured here; its estimated period is  $\sim 900$  yr.

09186+2944 A 221 Ba,Bb (HD 80101) has been discovered by R. Aitken in 1901; its 183 yr orbit presented here is still tentative. The visual component A (HJL 1054 AB) at  $343''$  is optical. However, the pair Ba,Bb contains a spectroscopic subsystem with a period of 52.8 days. *Gaia* does not provide the distance measurement. The dynamical parallax of 14.2 mas derived from the or-

bit matches the photometric distance.

09354+3958 COU 2084 Aa,Ab (HIP 47053). This is a quintuple system at 79 pc distance from the Sun. The outer  $25''$  pair A,B has an estimated period of 40 kyr. The component B (HIP 47054) is a 28 day spectroscopic binary, and the component Aa is also a tight spectroscopic and eclipsing pair with  $P = 1.07$  d and the primary of F2V spectral type. Our orbit of Aa,Ab with  $P = 50$  yr is well constrained. Note that the *Gaia* DR2 parallaxes of A and B are formally discordant ( $12.63 \pm 0.39$  and  $14.61 \pm 0.29$  mas, respectively), possibly being biased by the subsystems.

10454+3831 HO 532 A,C (HIP 52600). The orbit by Mante (2000) with  $P = 161$  yr, revised here to  $P = 326$  yr, is still poorly constrained. This is a nearby (13.6 pc) K7V dwarf. We do not confirm the  $0''.4$  subsystem CHR 191 A,B and believe that it is spurious. It has been resolved three times in the period from 1983 to 1991, at similar positions (Hartkopf et al. 1994), but subsequent speckle observations detected only the wide pair A,C, now at  $0''.7$  separation. The outer eccentricity  $e = 0.90$  is incompatible with a  $0''.4$  inner subsystem, violating dynamical stability. Orbits with smaller eccentricities or larger inclinations correspond to unrealistically small mass sum, so these parameters were fixed.

11017+3641 HDS 1574 Aa,Ab (HIP 53903). The new orbit with  $P = 47$  yr is relatively well defined. Comparison between *Gaia* and *Hipparcos* reveals  $\Delta\mu = (-1.3, -17.0)$  mas yr $^{-1}$  which matches the orbital motion of Aa,Ab. The companion B located at  $46''.8$  from A is also a close pair COU 1422 Ba,Bb with direct revolution (Aa,Ab is retrograde). Therefore, this is a quadruple system of 2+2 hierarchy with non-coplanar inner subsystems. We compute a preliminary orbit of Ba,Bb with  $P = 173$  yr.

11151+3735 CHR 192 Aa,Ab (HIP 54941) has a preliminary orbit with  $P = 200$  yr (Figure 3). The tertiary component at  $0''.6$  has been measured as well. This is a distant ( $\sim 300$  pc) triple system with a G5 giant primary component. We consistently measure smaller  $\Delta m$  at shorter wavelengths, indicating that Ab is hotter than Aa. *Gaia* measured a negative parallax, apparently being confused by the multiple nature of this source.

12089+2147 HDS 1714 Aa,Ab (HIP 59233) has moved almost on a straight line since its resolution by *Hipparcos* in 1991.25. The absence of significant  $\Delta\mu$  supports the long period of our preliminary orbit. The physical tertiary component B is at  $15''.3$ .

14353+4302 LSC 56 Aa,Ab (HIP 71366). The first tentative edge-on orbit with  $P = 11$  yr is determined here. The separation does not exceed 50 mas. We also measured the third star B at  $0''.5$ . The estimated period of A,B is  $\sim 400$  yr.

16147+3352 YSC 152 Ea,Eb (HIP 79551) belongs to the nearby (22.7 pc) quintuple system. The primary component (HIP 79607, GJ 615.2,  $\sigma$  CrB) is a 726 yr visual binary A,B with a 1.1 d subsystem Aa,Ab that has been resolved interferometrically. The pair Ea,Eb, at  $634''$  from AB, was known as a 52 yr astrometric binary (Heintz 1990). Here we determine the elements of its circular visual orbit with the same period. So far, the measurements of Ea,Eb cover only 10 years (owing to the large  $\Delta V \approx 3.3$  mag, this pair has not been resolved by *Hipparcos*). Comparison between the *Gaia* and *Hippar-*



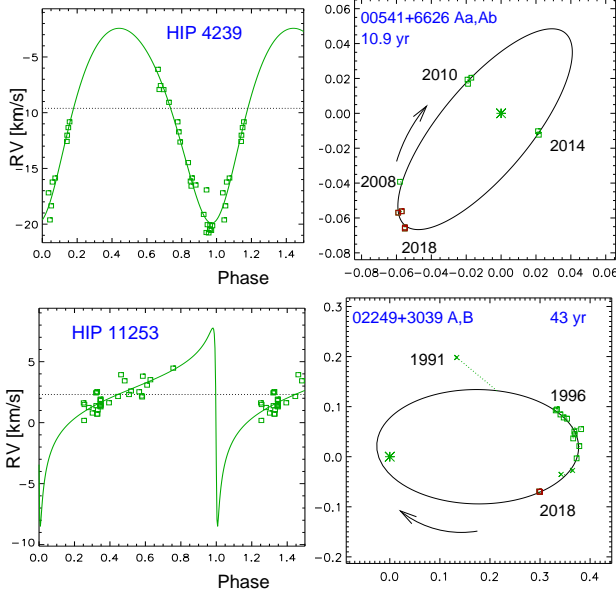


**Figure 5.** Combined spectro-interferometric orbits of HIP 4239 (top) and HIP 11253 (bottom). In this and following plots, the left panel shows the RV curve (green line and squares for the primary component, blue line and triangles for the secondary component). The right-hand panel shows orbits in the plane of the sky.

$\cos$  astrometry reveals  $\Delta\mu$  of the star E that matches its orbital motion and estimated mass ratio.

19514+4044 COU 2530 A,B (HIP 97706) is a quadruple system at 81 pc. The outer 4'4 pair AB,C (ORL 6) is confirmed by *Gaia*. We compute here the first visual orbit of the intermediate subsystem A,B with  $P = 55$  yr. Double lines in the spectrum reported by Guillout et al. (2009) suggest an inner subsystem Aa,Ab, but its orbit is unknown.

20599+4016 HDS 2989 Da,Db (HIP 103052, K7Ve, 41pc). We determined the preliminary orbit of Da,Db with  $P = 213$  yr. It has a common PM, parallax and RV with HIP 103641, located at projected separation of 20' (0.24 pc) from D. The component A itself is triple (a 2''2 visual binary with a 112 d spectroscopic subsystem). Although A and D are obviously related to each other, it is not clear at the moment whether they are gravitationally bound or are just members of some unknown moving group.

21308+4827 A 770 A,B. We computed a tentative edge-on orbit with  $P = 146$  yr. The outer companion at 1'1 is also measured; its estimated period is  $\sim 1$  kyr.

22139+3943. We computed a tentative orbit of McA 70 Aa,Ac (HIP 109754, K3III) and have not resolved the 0'09 subsystem Aa,Ab. We question the existence of Aa,Ab because it has not been confirmed by numerous speckle observations of Aa,Ac.

22359+3938 CHR 112 Aa,Ab (HIP 111546, B1Ve) is a distant (500 pc) pair. We compute its first orbit with  $P = 42$  yr, reasonably well constrained (grade 3). The visual components B at 22'3 and D at 81'6 have similar *Gaia* parallaxes and could be members of the same cluster, rather than components of a hierarchical system.

### 3.3. Combined visual-spectroscopic orbits

In this Section, we present orbits computed by fitting jointly positional measurements and radial veloci-

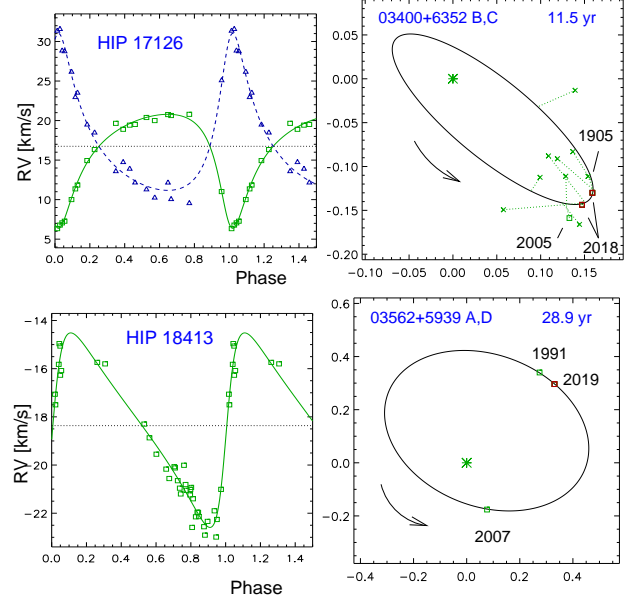


**Figure 6.** Combined spectro-interferometric orbit of HIP 17126 (top) and HIP 18413 (bottom).

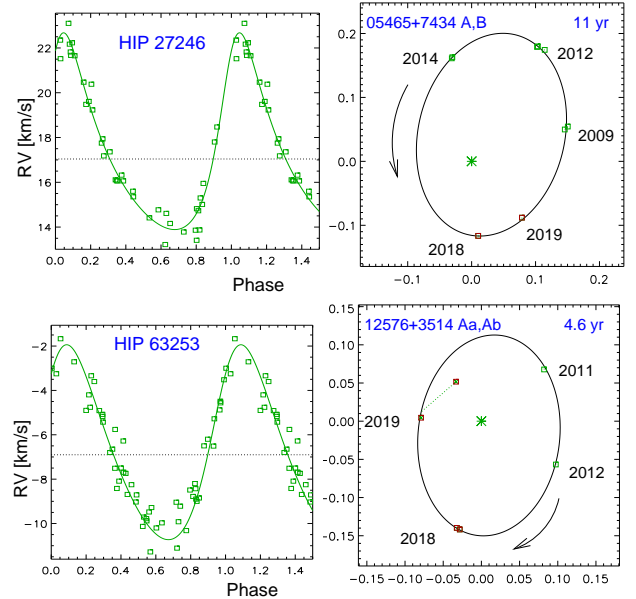


**Figure 7.** Combined spectro-interferometric orbits of HIP 27246 (top) and HIP 63253 (bottom).

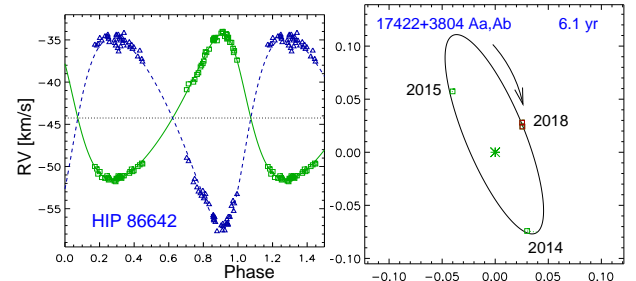


**Figure 8.** Combined spectro-interferometric orbit of HIP 86642.

**Table 6**  
Combined visual-spectroscopic orbits

WDS <i>HIP</i>	Disc.	$P$ (yr)	$T$ (yr)	$e$	$a$ (arcsec)	$\Omega_A$ (deg)	$\omega_A$ (deg)	$i$ (deg)	$K_1$	$K_2$ (km s <sup>-1</sup> )	$\gamma$
00541+6626 <i>4239</i>	YSC 19 Aa,Ab	10.868 ±0.060	2013.19 ±0.33	0.185 ±0.016	0.0718 ±0.0025	140.4 ±2.6	195.2 ±12.0	111.4 ±2.1	8.77 ±0.55	...	-9.60 ±0.38
02249+3039 <i>11253</i>	HDS 314 A,B	43.2 ±2.7	2026.5 ±2.5	0.89 fixed	0.271 ±0.070	214.8 ±31.2	110.3 ±12.4	133.5 ±24.2	6.29 ±1.44	...	2.25 ±0.63
03400+6352 <i>17126</i>	HU 1062 B,C	11.42 ±0.08	2000.601 ±0.055	0.475 ±0.016	0.146 ±0.002	232.4 ±1.1	157.8 ±2.9	70.0 fixed	7.22 ±0.14	9.95 ±0.36	16.76 ±0.10
03562+5939 <i>18413</i>	HDS 497 A,D	28.87 ±0.24	2006.630 ±0.143	0.456 ±0.009	0.442 ±0.048	246.7 ±1.6	264.6 ±2.8	51.2 ±5.0	4.04 ±0.08	...	-18.37 ±0.05
05465+7437 <i>27246</i>	YSC 148 A,B	11.140 ±0.039	1994.922 ±0.068	0.347 ±0.008	0.1638 ±0.0023	172.1 ±1.8	323.4 ±1.9	43.0 ±1.9	4.45 ±0.06	...	17.07 ±0.04
12490+6607 <i>62556</i>	DEL 4 Aa,Ab	0.14810 ±0.00001	1993.3055 ±0.0012	0.080 ±0.004	...	...	135.1 ±3.0	...	21.80 ±0.20	22.36 ±0.22	...
12490+6607	DEL 4 A,B	7.370 ±0.013	1994.490 ±0.022	0.511 ±0.012	0.356 ±0.007	201.5 ±0.7	263.4 ±0.7	78.1 ±0.7	5.22 ±0.14	10.80 ±0.31	-10.67 ±0.06
12576+3514 <i>63253</i>	BWL 53 Aa,Ab	4.595 ±0.096	2010.26 ±0.10	0.184 ±0.015	0.133 ±0.005	352.4 ±2.4	314.6 ±7.0	134.7 ±3.9	4.39 ±0.15	...	-6.90 ±0.08
13198+4747 <i>65026</i>	HU 644 A,B	49.077 ±0.07	2017.400 ±0.45	0.221 ±0.004	1.551 ±0.005	271.0 ±0.1	253.1 ±0.3	94.31 ±0.05	1.07 ±0.10	...	0.96 ±0.06
13198+4747	CHR 193 Aa,Ab	1.22765 ±0.00016	2014.909 ±0.022	0.067 ±0.006	0.1115 ±0.0020	279.8 ±0.9	356.0 ±6.5	87.7 ±1.0	8.703 ±0.094	...	...
17247+3802 <i>85209</i>	HSL 1 Aa,Ab	1.22496 ±0.00010	1986.381 ±0.002	0.160 ±0.002	0.0290 ±0.0009	53.2 ±1.7	358.3 ±0.9	81.5 ±3.3	16.30 ±0.11	17.44 ±0.13	...
17247+3802	HSL 1 Aab,Ac	34.17 ±0.48	2011.39 ±0.72	0.148 ±0.011	0.306 ±0.019	57.8 ±0.2	277.2 ±1.1	92.7 ±0.2	3.62 ±0.20	7.32 ±0.78	0.18 ±0.04
17422+3804 <i>86642</i>	RBR 29 Aa,Ab	6.114 ±0.009	2008.475 ±0.015	0.260 ±0.004	0.1033 ±0.017	203.1 ±5.9	53.7 ±1.0	105.8 ±3.4	8.61 ±0.03	11.25 ±0.07	-44.25 ±0.03

ties (RVs). Their elements are given in Table 6. The RV curves and orbits in the plane of the sky are plotted in Figures 5 to 8. Each system is commented below except HIP 62556, 65026, and 85209 discussed in the following Sections.

00541+6626 YSC 19 Aa,Ab (HIP 4239). Its first orbit is defined independently by both positional measurements and the CfA RVs covering a time span of 16 yrs. The combined elements are quite accurate,  $P = 10.87 \pm 0.06$  yr (Figure 5, top). The *Gaia* parallax of  $9.49 \pm 0.05$  mas corresponds to the mass sum of  $3.7 M_{\odot}$ , in rough agreement with the expected mass of two F0V stars (Aa and Ab are similar,  $\Delta m = 0.4$  mag). Lines of the secondary component Ab are detectable, but their RVs do not match the expected RVs in the 11-yr orbit, so Ab may contain a subsystem. We use here only the RVs of Aa. The *Gaia*  $\Delta\mu$  is small, only  $\sim 0.1$  of the orbital motion, with opposite direction as expected. The outer physical component B at  $0''.9$  moves slowly with an estimated period of  $\sim 500$  yr.

02249+3039 HDS 314 Aa,Ab (HIP 11253, HD 14784). The orbit of Ling (2012) with  $P = 82.18$  yr does not agree well with recent measurements and, moreover, yields an unrealistically small mass sum. Its adjustment using only relative astrometry does not help; the first *Hipparcos* resolution obviously deviates from the remaining measurements. However, use of the RVs improves the situation, although they do not cover the full period. To the 34 RVs measured with the CfA Digital Speedometers between 1993 and 2009 we added one more from TRES obtained in 2009, as well as the mean RV reported by *Gaia*. The resulting orbit (Figure 5, bottom) has a large eccentricity of  $e = 0.89$  and is still not fully constrained, although the mass sum is now realistic. Further monitoring of this pair by both speckle interferometry and RVs as it approaches the periastron, predicted for 2026, will

eventually lead to a reliable orbit. This is a quadruple system with a 2+2 hierarchy at 55 pc from the Sun (the component C, at  $20''.4$  from A, is itself a  $0''.6$  pair).

03400+6352 HU 1062 B,C (HIP 17126) forms a physical pair with the component A (HIP 17118), at  $45''.7$  distance from each other. Both stars have common parallaxes ( $23.27 \pm 0.030$  mas for A), PMs, and RVs. The period of A,B is  $\sim 50$  kyr. The pair B,C has been resolved in 1905 at  $0''.19$ , but its visual micrometer measurements accumulated during the past century were too rare and discordant for orbit determination. Prior to our observations at WIYN, only one speckle measurement has been made in 2005. On the other hand, the RV monitoring at CfA revealed B,C as a double-lined binary with a period of  $\sim 11$  yr. The combined orbit in Figure 6, top, was computed by fixing the inclination to  $i = 70^\circ$  to bring the RV amplitudes in agreement with estimated masses of B and C ( $1.0$  and  $0.8 M_{\odot}$ , respectively) and with the mass sum of  $1.87 M_{\odot}$  deduced from the parallax. Further high-resolution observations of B,C are needed to cover the full orbit and constrain its inclination. The  $\Delta\mu$  of the unresolved star BC measured by *Gaia* and *Hipparcos*, ( $+8.1, +2.6$ ) mas yr<sup>-1</sup>, is opposite to the orbital speed of C relative to B, ( $-48, -31$ ) mas yr<sup>-1</sup> in 2015.5.

03562+5939 (HIP 18413, HD 24409, GJ 3257) is a pair of dwarfs at a distance of 22.7 pc from the Sun; it belongs to the 25-pc sample of solar-type stars. The pair A,D was first resolved by *Hipparcos* (HDS 497 A,D). The RVs were monitored by D. L. using the CfA RV spectrometers from 1993.1 to 2008.2, a total of 36 measurements. We also used one RV from TRES and the mean RV measured by *Gaia*. A preliminary period of 28 yrs has been determined from the RVs. Positional measurements are available only at three epochs: 1991.25, 2007.6, and 2018.9. Nevertheless, the combined orbit in

Figure 6, bottom, is defined reasonably well if the quadrant in 2007.6 is changed. The rms residuals in RV are  $0.41 \text{ km s}^{-1}$ . At the *Gaia* epoch of 2015.5, the companion moved on the orbit with a speed of  $(+18, +49) \text{ mas yr}^{-1}$ , two times faster and in opposite direction compared to  $\Delta\mu = (-10.6, -25.0) \text{ mas yr}^{-1}$  measured by *Gaia* and *Hipparcos*. This confirms the orbit and indicates comparable masses of A and D, despite substantial magnitude difference ( $\Delta m = 3.4 \text{ mag}$  in the *V* band). Lines of the secondary component D are not detected in the spectra, but they could reduce the RV amplitude by blending with the lines of A. The RV amplitude and the estimated mass of A,  $1.0 M_{\odot}$ , correspond to the minimum mass of  $0.64 M_{\odot}$  for D. The faint tertiary companion E at  $9''.5$  (BUP 48 A,E) is physical. The distant companions B and C listed in the WDS are optical.

05465+7437 (YSC 128 A,B; HIP 27246, distance 39 pc) was resolved for the first time in 2009.75 by Horch et al. (2012) at  $0''.15$ . Its RVs measured from 1987.3 to 1999.9 are published by Latham et al. (2002) who also derived the spectroscopic orbit; we do not copy these RVs in Table 5. By combining RVs with positional measurements at six epochs (including two from this program), we derive an excellent combined orbit (Figure 7, top) with a period of  $11.14 \pm 0.05 \text{ yr}$ . An astrometric orbit with similar period has been published by Jancart et al. (2005). The tertiary companion C is located at  $10''.9$ . Its parallax of  $26.80 \pm 0.04 \text{ mas}$  is measured by *Gaia* more accurately than the parallax of AB. The mass sum derived from the orbit and the parallax is  $1.82 M_{\odot}$ ; it matches the masses of A and B estimated from the luminosity, as well as the secondary mass computed from the RV amplitude and inclination.

12576+3514 (HIP 63253, GJ 490) is a low-mass quadruple system of M dwarfs at 20 pc from the Sun. The outer  $16''$  pair LDS 5764 A,B has been known since 1950. Another star C with a similar PM, at  $12''.7$  from A, is unrelated according to its *Gaia* parallax. Bowler et al. (2015) resolved in 2011 stars A and B into tight pairs Aa,Ab and Ba,Bb with separations of  $0''.13$  and  $0''.17$ , respectively. We measured both subsystems in 2018 and re-observed them in 2019. The observations in 2019 were repeated twice on the same night because on the first attempt the results were affected by telescope vibration. We obtained different position angles of Aa,Ab on this night and consider both our measurements uncertain, given the small  $0''.06$  separation and the large  $\Delta m \sim 3 \text{ mag}$ . On the other hand, the measurements of Ba,Bb on that night are mutually consistent.

A spectroscopic orbit of Aa,Ab with a period of 4.6 yr was derived by one of us (G. T.) from 45 RVs measured with the CfA Digital Speedometers between 1984 and 2008. We use these RVs and the 11 RVs from Sperauskas et al. (2019) to derive the combined orbit (Figure 7, bottom). The weighted rms RV residuals are  $0.60 \text{ km s}^{-1}$ . Despite the short period, the RV amplitude is moderate,  $K_1 = 4.4 \text{ km s}^{-1}$ , because the orbit has an inclination of  $135^\circ$ . Our discordant measurements in 2019 are assigned a very low weight. We adopt the *Gaia* parallax of the component B,  $49.57 \pm 0.13 \text{ mas}$ , as the distance to the system because the parallax of A,  $46.83 \pm 0.28 \text{ mas}$ , is less accurate. The mass sum of Aa,Ab is then  $0.90 M_{\odot}$ . Our relative photometry,

$\Delta V_{\text{Aa,Ab}} = 3.2 \text{ mag}$ , is consistent with  $\Delta K_{\text{Aa,Ab}} = 1.69 \text{ mag}$  measured by Bowler et al. (2015). The absolute magnitudes of Aa and Ab correspond to dwarfs with masses of 0.60 and  $0.30 M_{\odot}$ , matching the orbit. The RV amplitude and inclination also match these masses. The *Gaia* astrometry supports our orbit of Aa,Ab by measuring  $\Delta\mu = (32.6, 10.4) \text{ mas yr}^{-1}$ . The computed speed of orbital motion in 2015.5 is  $(-125.5, -63.8) \text{ mas yr}^{-1}$ . The ratio of those speeds equals the wobble factor  $f \approx 0.24$ , in agreement with the calculated  $f = 0.27$ .

The pair Ba,Bb is fainter than A,  $V_{\text{Ba,Bb}} = 13.2 \text{ mag}$ . The separation corresponds to a period of  $\sim 10 \text{ yr}$ ; we observed the motion of Ba,Bb pair by  $24^\circ$  in one year. The orbit of Ba,Bb can be determined with a few more measurements. We also derived 45 RVs of the star B from the CfA and TRES spectra taken between 1984 and 2015. Owing to the faintness of the star B, the errors are large, from 3 to  $5 \text{ km s}^{-1}$ , and we do not resolve the double lines; the mean RV of B is  $-5.8 \text{ km s}^{-1}$ . As no orbit of Ba,Bb could be derived yet from these RVs, they are not presented here.

17422+3804 (HIP 86642, HD 161613, distance 42 pc) is a solar-type triple system. The double-lined spectroscopic and astrometric orbit of the inner pair RBR 29 Aa,Ab with  $P = 6.1 \text{ yr}$  has been recently published by Fekel et al. (2018); we do not copy these RVs in Table 5. Measurements in the plane of the sky in 2013.8 and 2015.5 are available from Roberts et al. (2015). We resolved the pair in 2018.47 but did not resolve it in 2018.65. The elements of our combined orbit (Figure 8) do not differ substantially from the published orbit and, therefore, confirm its astrometric elements. The RV amplitudes and inclination imply the masses of 1.02 and  $0.79 M_{\odot}$  which match the masses estimated from the absolute magnitudes. The orbital parallax of  $25.3 \text{ mas}$  is to be preferred over the *Gaia* parallax of  $23.94 \pm 0.11 \text{ mas}$  because the latter is likely biased by the binary. The ratio of astrometric and full semimajor axes,  $f = 0.293$ , implies the mass ratio  $q = f/(1-f) = 0.42$  if the secondary component Ab has a large  $\Delta m$ . The outer  $2''.2$  pair A,B has an estimated period of  $\sim 600 \text{ yr}$ .

#### 3.4. HIP 62556, a triplet of M3V dwarfs

This triple star, located at 10 pc from the Sun, is designated as HIP 62556, GJ 487, WDS J12490+6607, and BP Dra. The inner spectroscopic subsystem Aa,Ab with  $P = 54 \text{ d}$  has been studied by Delfosse et al. (1999). The estimated semimajor axis of 23 mas makes it resolvable at 8-m class telescopes or with the CHARA array but, so far, it has never been resolved by speckle. However, these authors resolved in 1997 the outer subsystem A,B (DEL 4) at  $0''.23$ . They noted that the spectrum is triple-lined and that the outer period is  $\sim 3000 \text{ days}$ . Available astrometry and two measurements at WIYN define the outer visual orbit with  $P = 7.4 \text{ yr}$ .

This system has been observed with the CfA spectrometers 79 times, from 1984 to 2003. These data cover 2.6 outer periods and allow us to determine the masses and distance from the combined outer orbit. We used the TRICOR software and the spectrum of GJ 725B as a template to derive the RVs of three stars Aa, Ab, and B. Their relative fluxes at  $5187 \text{ \AA}$  are 1:0.97:0.73. The in-

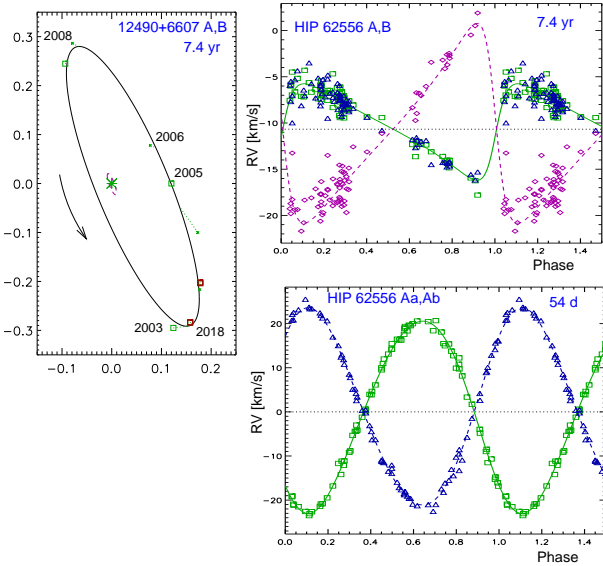


**Figure 9.** Orbits of the inner and outer pairs in HIP 62556 (GJ 487).

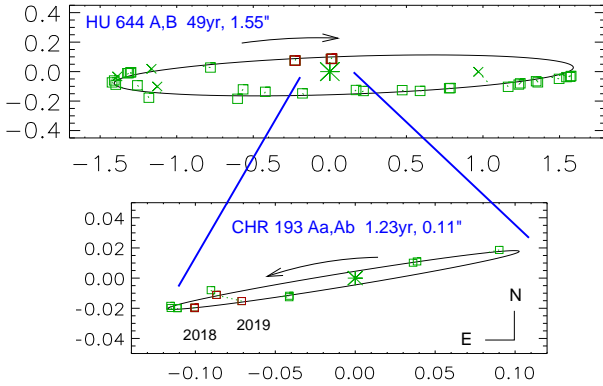


**Figure 10.** Orbits of HIP 65026 (WDS J13198+4747) computed independently. The upper panel shows the outer system HU 644 A,B; the lower panel shows the inner subsystem CHR 193 Aa,Ab.

ner subsystem is not resolved and does not cause wobble in the outer orbit because Aa and Ab are nearly equal. The combined orbit is shown in Figure 9. The rms RV residuals are 0.68, 0.91, and 1.39 km s<sup>-1</sup> for Aa, Ab, and B, respectively.

As the outer inclination is known, we determine the masses of A and B as 0.52 and 0.25  $M_{\odot}$ . The inner mass ratio  $q_{Aa,Ab} = 0.97$  defines the masses of Aa and Ab, 0.26  $M_{\odot}$  each. The inner RV amplitudes then correspond to the inner inclination of 77°, so the orbits are, most likely, coplanar. The mass sum and outer semimajor axis imply an orbital parallax of 103 mas. The *Hipparcos* parallax is  $97.9 \pm 1.8$  mas, while *Gaia* does not yet provide astrometry of this complex and fast triple system.

### 3.5. The low-mass triple system HIP 65026

This triple system is known as HIP 65026, HD 115953, GJ 508, ADS 8861, WDS J13198+4747, and BD+48 2108. Simbad gives the spectral type M2V and contains 102 references. The *Gaia* DR2 parallax is  $109.98 \pm 0.83$  mas (distance 9 pc), and the proper motion is  $(+226.5, -23.8)$  mas yr<sup>-1</sup>.

The visual binary HU 644 A,B was discovered in 1904.

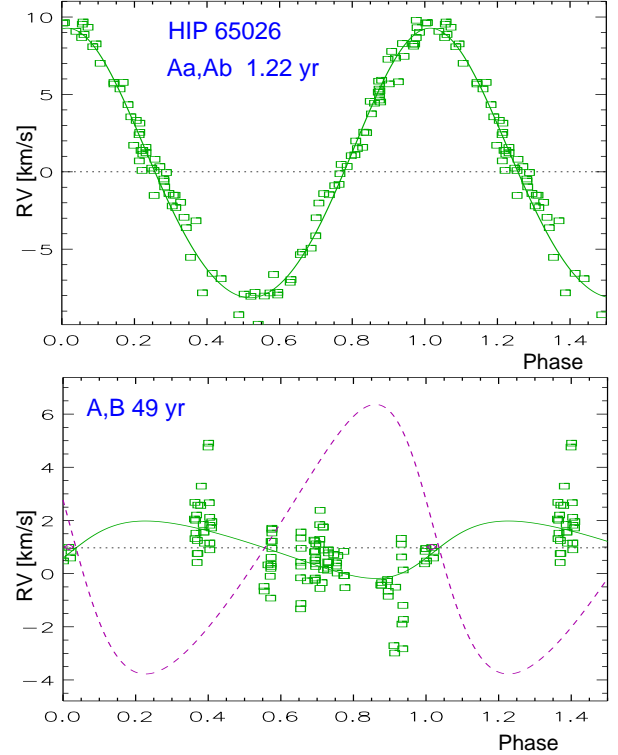


**Figure 11.** RV curves of the inner (top) and outer (bottom) orbits of HIP 65026 from the combined solution. In each curve, the contribution of other orbit is subtracted. The dotted line in the lower plot shows the expected RV curve of the component B.

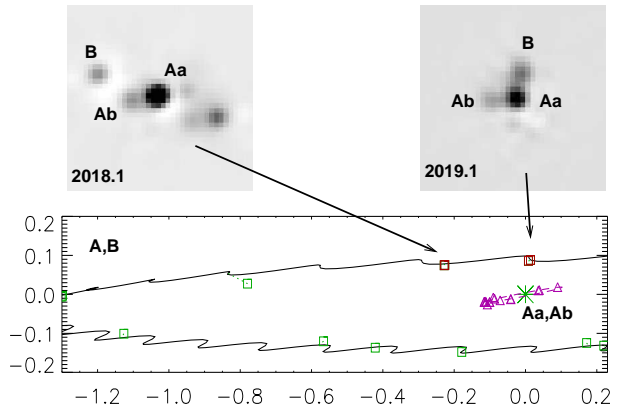


**Figure 12.** Fragment of the outer and inner orbits of HIP 65026 and the reconstructed images of the triple star recorded with the red NESSI camera in 2018 (separations 0''.24 and 0''.10) and in 2019 (separations 0''.09 and 0''.08), when the previously unobserved part of the outer orbit was covered. The wavy line shows the wobble produced by the inner subsystem.

It has made 2.3 revolutions on its 49 yr orbit, which is now very well defined (grade 2). The inner subsystem CHR 193 Aa,Ab was discovered in 1992.3 at 0''.11 separation by Hartkopf et al. (1994) and has been measured several times since. Independently, the RV variation was found by Tokovinin & Smekhov (2002) (observations in 1995, 1996, and 2000) and by Sperauskas et al. (2019) (2011 to 2018). The latter authors computed a spectroscopic orbit with a period of 447 days (1.22 yr) which refers to the inner pair Aa,Ab. Beuzit et al. (2004) resolved the triple system using adaptive optics and an-

nounced a preliminary spectroscopic orbit of the inner pair with  $P = 450$  d that has not been published so far. Beuzit et al. wrote that the spectra are triple-lined.

As a first step, the outer and inner orbits were analyzed separately (Figure 10). We fit the outer orbit using all available data, but then fix the outer period to 49.077 yr and fit the remaining elements using only speckle and adaptive optics data. Both orbits have a large inclination. The inner orbit uses the RVs mentioned above and additional 87 unpublished RVs measured with the CfA spectrometers between 1995.5 and 2006.4. Owing to the long RV coverage, the inner period is very accurate.

The two orbits were then fitted simultaneously using the IDL code `orbit3.pro` (Tokovinin & Latham 2017). Only interferometric measurements of the outer pair are used, and its period, determined by the long-term visual coverage, is kept fixed. The resulting elements are listed in Table 6. The global weighted rms residuals in position are 5 mas for the inner and outer subsystems. However, some observations of the outer pair left unrealistically large residuals of almost 30 mas and caused divergence of the combined fit. They were carefully examined and re-weighted. The measurements in 1989.13, 2000.32, 2005.235, 2005.32, and 2013.29 were ignored, while some other data were assigned errors larger than usual. The RV residuals are  $0.72 \text{ km s}^{-1}$ . The results of the joint solution are very similar (mostly within the errors) to the orbits computed separately. The RV curves are presented in Figure 11. The combined fit defines additional parameter, the wobble factor  $f_{Aa,Ab} = 0.425 \pm 0.025$  (ratio of the wobble amplitude to the inner axis). The wobble amplitude is 49 mas. Figure 12 shows a fragment of the outer orbit with wobble and the reconstructed high-resolution images obtained at WIYN. They cover previously unobserved part of the outer orbit.

The nodes of both orbits are known from the RVs, allowing us to compute the angle between the orbital angular momenta (relative inclination) of  $11^\circ 3 \pm 1^\circ 0$ . The orbits are almost, but not quite, coplanar, and have small eccentricities. Intriguingly, the period ratio is  $39.97 \pm 0.005$ , suggesting that the orbits may be in a weak mean motion resonance. Such architecture is found in some other low-mass triple system and hints at their origin in a common disc (Tokovinin 2018c).

The *Gaia* parallax of  $109.98 \pm 0.83$  mas is likely biased by the astrometric subsystem with a period of 1.2 yr, not accounted for in the DR2 astrometric solution (the large parallax error shows its poor quality). The components' masses derived from the orbits and the *Gaia* parallax do not quite match the absolute magnitudes. We adopt here the parallax of 101 mas computed from the outer orbit and the estimated masses of Aa, Ab, and B, 0.58, 0.42, and  $0.48 M_\odot$  respectively (sum  $1.51 M_\odot$ ). With this parallax, the components are located on the main sequence. To match this model, the axis of the inner orbit should be larger than measured by 4%, while its formal error is 1.8%. Considering the difficulty of measuring the inner pair in this triple system, such disagreement is not alarming.

We determine  $V = 9.33, 10.83, 10.21$  mag for Aa, Ab, and B using published and new differential photometry together with the combined magnitude  $V_{\text{tot}} = 8.76$  mag. The wobble factor computed from the above masses and magnitudes is  $f_{Aa,Ab} = 0.44$  for resolved measurements

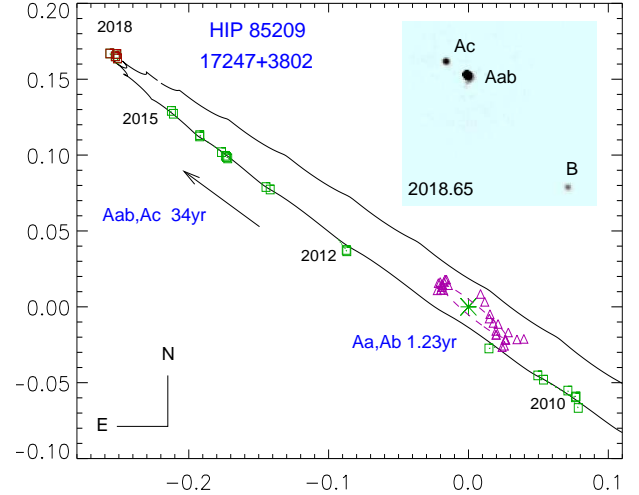


**Figure 13.** Visual orbits of HIP 85209 (WDS J17247+3802). Fragment of the outer orbit and the inner orbit are plotted to scale. The insert shows the reconstructed speckle image in 2018.65 in the red channel with components Ac and B (the inner pair Aa,Ab is unresolved).

of Aa,B and  $f_{Aa,Ab} = 0.24$  for photo-center measurements of A,B in the  $V$  band; the measured wobble factor is 0.42. Similarly, the wobble factor of the outer orbit would be 0.33 (resolved) and 0.07 (photo-center). Heintz (1969) determined the photo-center wobble of the outer orbit as  $f_{A,B} = 0.088$ . At that time, the existence of the one-year subsystem Aa,Ab was not known, so Heintz derived a biased parallax of  $119 \pm 3.5$  mas.

The masses, period, and inclination of the outer system allow us to compute the RV amplitudes of  $3.6$  and  $5.1 \text{ km s}^{-1}$  for A (center-of-mass) and B, respectively. Yet, the free fit yields a much smaller outer amplitude  $K_1 = 1.07 \text{ km s}^{-1}$ . We tentatively attribute the discrepancy to blending with other components that reduces the amplitude.

The study of this remarkable low-mass triple system will further benefit from spectroscopy with a higher resolution and, possibly, at longer wavelengths to resolve spectrally all three stars and determine their unbiased RV amplitudes. High inclination of the orbits favors measurement of the orbital parallax. Meanwhile, future *Gaia* releases should include orbital motion in the astrometric model, delivering accurate astrometric orbits and unbiased parallax.

### 3.6. The quadruple system HIP 85209

17247+3802 (HIP 85209, HD 157948) is a quadruple system of 3+1 hierarchy located at 50 pc from the Sun. The outer  $1''.8$  pair COU 1142 A,B is known since 1974; its estimated period is  $\sim 500$  yr. On the other hand, this is a double-lined spectroscopic binary with a period of 448.6 days (Goldberg et al. 2002). This pair, denoted in WDS as HSL 1 Aa,Ab, has been resolved by both the fine-guided sensors of the Hubble Space Telescope (Heasley et al. 2002; Horch et al. 2006) and by speckle interferometry, allowing Horch et al. (2015a) to determine its visual elements. Speckle interferometry also revealed an intermediate subsystem Aab,Ac (HSL 1 Aab,Ac) at  $0''.3$  separation. Its first orbit with  $P = 122$  yr and a large eccentricity of  $e = 0.72$  computed by

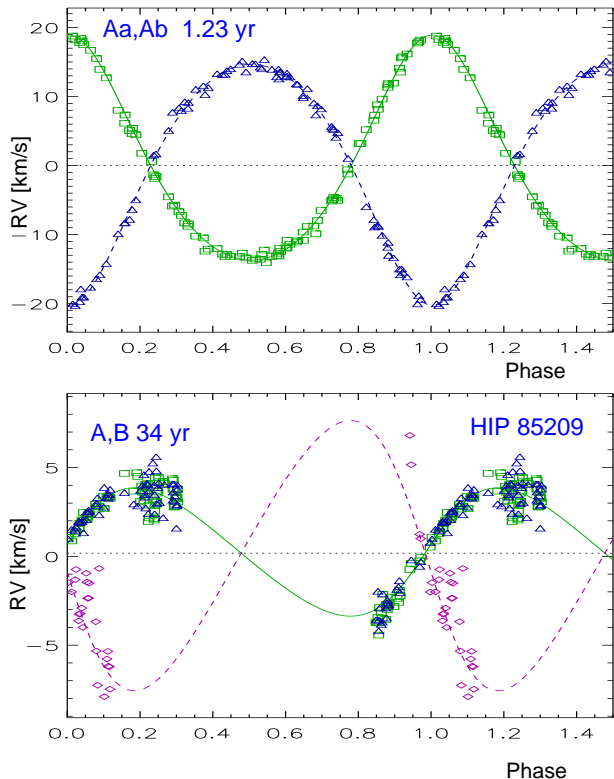


**Figure 14.** RV curves of the inner (top) and outer (bottom) orbits of HIP 85209 from the combined solution. In each curve, the contribution of other orbit is subtracted.

Roberts & Mason (2018) does not agree with the latest observations that cover now 17 years and suggest a quasi-circular orbit with  $P \approx 38$  yr.

To gain a better understanding of this system, we fitted the inner and middle orbits simultaneously using the latest measurements by Horch et al. (2019) in addition to the published and our own astrometry and the RVs from Goldberg et al. (2002). Their measurements, covering the period from 1982.5 to 1987.5, are reprocessed and extended to 2009. Furthermore, the spectra from TRES obtained from 2009.4 to 2015.4 were processed by TRICOR, extracting the RVs of Aa, Ab, and Ac. The RV data therefore cover almost entire outer period of 34 yr, constraining the outer orbit. The elements of both orbits fitted jointly are given in Table 6 and illustrated in Figures 13 and 14. The inner spectroscopic elements differ only slightly from the published orbit; the weighted rms residuals in RV are 0.19, 0.37, and 1.92 km s<sup>-1</sup> for Aa, Ab, and Ac, respectively. The resulting masses of Aa and Ab are 0.91 and 0.85  $M_{\odot}$ . The *Gaia* parallax of 20.676±0.11 mas for the component B (it is more accurate than the parallax of A) and the inner orbit lead to the mass sum of 1.84  $M_{\odot}$  that agrees with the spectroscopic masses. The outer orbit correspond to the mass sum of 2.77  $M_{\odot}$ . However, the RV amplitudes in the outer orbit imply smaller masses of 1.20 and 0.57  $M_{\odot}$  for Aa+Ab and Ac, respectively. This means that the RV amplitudes in the outer orbit are slightly underestimated, possibly because the RVs measured by TRICOR are biased by blending in the triple-lined spectra.

The components Aa and Ab are similar in both mass and brightness. Using the *Gaia* photometry  $V_A = 8.08$  mag,  $\Delta V_{Aa,Ab} = 0.4$  mag (in rough agreement with

**Table 7**  
Newly resolved pairs

WDS	HR	$\rho$ (arcsec)	$\theta$ (deg)	$\Delta m(562)$ (mag)	$\Delta m(716)$ (mag)
00585+6621	273	1.47	58	6.1	5.7
01029+4121	290	0.10	143	2.0	1.5
04551+5516	1555	0.05	155	0.2	0.2
13057+3548	4943	0.22	63	4.1	4.2

Horch et al. 2019), and  $\Delta m_{Aa,Ab} = 3.0$  mag measured here, we get the individual  $V$  magnitudes of 8.72, 9.12, and 11.17 mag for Aa, Ab, and Ac. Their absolute magnitudes and the masses measured here match standard relations for main-sequence stars. This star has been considered to be metal-poor. However, given the composite nature of the spectrum, its standard analysis may lead to biased results. The kinematics does not distinguish HIP 85209 from the population of Galactic disk.

The inner and middle orbits are seen nearly edge-on; their relative inclination is  $12^{\circ}0 \pm 3^{\circ}0$ . The position angle of the pair A,B ( $221^{\circ}$ ) is close to the position angle of both inner orbits, while the observed motion of A,B is mostly radial (increasing separation), suggesting that the orbit of A,B can be oriented approximately in the same plane. Therefore, this is a 3+1 “planetary” hierarchy with quasi-coplanar and quasi-circular orbits.

### 3.7. New binaries

Four reference stars were unexpectedly resolved as binaries. Table 7 lists these objects, while all their measurements are found in the main Table 1. Three stars with a large  $\Delta m$  still provide useful references in the data processing because the binary signature is automatically removed from the reference power spectrum by our pipeline.

Two newly resolved pairs are in fact triple systems. The new 1''47 companion to HR 273 (HIP 4572, HD 5550, A0III, 110 pc) is found in the *Gaia* DR2 at a similar position, 1''455 and 58°4. Considering the PM of 45 mas yr<sup>-1</sup>, we conclude that this companion is physical (co-moving). Meanwhile, the star A is a chemically peculiar double-lined spectroscopic binary with a period of 6.82 d according to Carrier et al. (2002). Therefore, this is a new triple system hosting a close inner pair.

HR 1555 (HIP 22854, HD 30958, ADS 3508, B9.5V, 236 pc) is a known visual binary BU 1187 with a separation of 12''7. *Gaia* astrometry confirms that this binary is physical (common PM and parallax). Its main component A is resolved here into a tight pair Aa,Ab; the separation of 47 mas implies a short orbital period of  $\sim 15$  yr. Indirectly, this pair is confirmed by the astrometric acceleration,  $\Delta\mu = (-2.6, -3.6)$  mas yr<sup>-1</sup>. The orbit of Aa,Ab can be determined within several years.

### 3.8. Spurious pairs

Some subsystems are not confirmed by subsequent observations. It is important to recognize these cases for cleaning up the statistics of hierarchical multiplicity. However, it is much easier to discover a subsystem than to prove its non-existence because a negative observation does not necessarily mean that the subsystem is spurious. It could have closed down below the resolution limit or

**Table 8**  
Unconfirmed subsystems

WDS	Discoverer code	$\rho$ (arcsec)	Last (yr)	$P^*$ (yr)
02132+4414	CHR 5	0.2	1987	80
03127+7133	SCA 171 Aa,Ab	0.4	2009	60
03492+2408	CHR 125 Aa,Ab	0.2	1991	60
04184+2135	LMP 52 Aa,Ad	0.3	2000	40
04493+3235	CHR 19	0.04	1984	5
09068+4707	COU 2687	0.45	1993	100
09188+3648	CHR 173 Ba,Bb	0.24	2004	15
10454+3831	CHR 191 A,B	0.36	1991	15
16238+6142	CHR 138 Aa,Ab	0.2	1990	90
17491+5047	CHR 65 Aa,Ab	0.12	1985	11
18443+3940	CHR 77 Ca,Cb	0.10	2005	20
19111+3847	STF 2481 Aa,Ab	0.1	2012	10
22139+3943	BNU 8 Aa,Ab	0.19	2005	60
23439+3232	BAG 30 Ba,Bb	0.2	2000	10
23460+4625	MCA 75 Aa,Ab	0.2	2003	75

the contrast may exceed the dynamic range of the technique. A crude estimate of an orbital period  $P^*$  based on the projected separation (assuming it equals the semi-major axis) helps to evaluate the veracity of subsystems. We also considered other evidence such as astrometric acceleration, RV variability, and observations of outer subsystems.

Table 8 lists likely spurious subsystems unresolved at WIYN. Its first two columns provide the WDS codes and discoverer designations. The latest measured separations and the epochs of the last reported resolution are given in the following two columns. The last column gives the period estimate.

The existence of inner and outer subsystems with comparable separations is highly improbable because such triples would be dynamically unstable, unless their configuration is a result of projection. When the outer orbit is known, the projection is no longer relevant and we can confidently rule out spurious inner pairs. This is the case of 03127+7133 (outer period 583 yr according to our updated orbit), 10454+3831 (outer period 326 yr), and 22139+3943 (outer period 125 yr). Another spurious “trapezium” triple is 23460+4625.

#### 4. SUMMARY

Our observations make an incremental contribution to the data on hierarchical multiple systems. Astrometric measurements at WIYN will help to determine orbits of many subsystems in the future, while several orbits are computed here. Mostly they refer to low-mass and nearby hierarchies. Our work also contributes differential photometry in two passbands. We discovered serendipitously two new triple systems and confirmed the spurious nature of some previous resolutions.

Low-mass hierarchies are often found in “planetary” configurations, where the inner and outer orbits are approximately co-planar, the pairs are co-rotating, and the orbital eccentricities are moderate, like in HD 91962 (Tokovinin et al. 2015). Two such systems, HIP 65026 and 85209, are studied here in detail. We accurately measured mutual orbit inclinations in both systems, proving their approximate co-planarity. They also have moderate eccentricities, presumably being sculpted by dissipative evolution in accretion disks. Despite similarities with planetary systems, however, stellar hierarchies have less

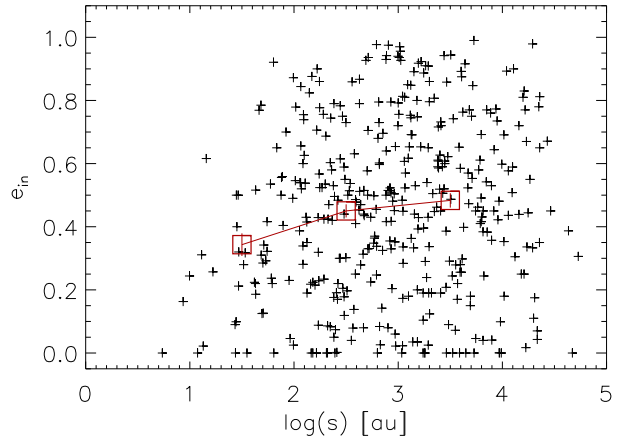


**Figure 15.** Eccentricity of inner visual orbits in hierarchical systems vs. projected separation  $s$  of their outer components. The red squares with error bars plot mean eccentricities and their errors in the separation bins of one dex.

coplanar and more eccentric orbits.

However, not all subsystems have quasi-circular orbits. Quite to the contrary, nearly half of the orbits in Table 3 (13 out of 23) have eccentricities exceeding 0.5. Large eccentricities suggest an important role of dynamical interactions in shaping the architecture of these hierarchies. In this case, the eccentricities are expected to follow the thermal distribution  $f(e) = 2e$  and the mutual orbit inclinations in triple systems should be random (uncorrelated). Nearly orthogonal orbits should further increase the eccentricities of inner subsystems through Kozai-Lidov oscillations.

It is likely that the role of dynamical interactions increases at larger spatial scales. To probe this idea, we plot in Figure 15 eccentricities of inner visual orbits in hierarchical systems versus projected separation  $s$  of the outer components, based on the current version of the MSC. We made no attempt to filter the quality of 397 visual orbits in this plot (including the orbits determined here) and caution that the MSC is burdened by numerous selection effects. Nevertheless, a trend of smaller inner eccentricities at projected outer separations  $s < 100$  au is emerging. As noted by Tokovinin (2017), compact hierarchies also tend to have more aligned orbits. Further accumulation of data on orbits in hierarchical stellar systems, especially in compact ones, will help to clarify these trends.

Observations in the paper made use of the NN-EXPLORE Exoplanet and Stellar Speckle Imager (NESSI). NESSI was funded by the NASA Exoplanet Exploration Program and the NASA Ames Research Center. NESSI was built at the Ames Research Center by Steve B. Howell, Nic Scott, Elliott P. Horch, and Emmett Quigley. This project is partially supported by the NASA award #1598596. B. Mason has kindly commented the draft version of our paper.

This work used the SIMBAD service operated by Centre des Données Stellaires (Strasbourg, France), bibliographic references from the Astrophysics Data System maintained by SAO/NASA, and the Washington Double Star Catalog maintained

at USNO. This work has made use of data from the European Space Agency (ESA) mission Gaia (<https://www.cosmos.esa.int/gaia>) processed by the Gaia Data Processing and Analysis Consortium (DPAC, <https://www.cosmos.esa.int/web/gaia/dpac/consortium>). Funding for the DPAC has been provided by national institutions, in particular the institutions participating in the Gaia Multilateral Agreement.

*Facilities:* WIYN.

## REFERENCES

- Alonso-Floriano, F. J., Caballero, J. A. Cortés-Contreras, M et al. 2015, *A&A*, 583, 85
- Beuzit, J.-L., Ségransan, D., Forveille, T. et al. 2004, *A&A*, 425, 997
- Bowler, B. P., Liu, M. C., Shkolnik, E. L., & Tamura, M. 2015, *ApJS*, 216, 7
- Brandt, T.D. 2018, *ApJS*, 239, 31
- Carrier, F., North, P., Udry, S. & Babel, J. 2001, *A&A*, 394, 151
- Delfosse, X., Forveille, T., Beuzit, J.-L. et al. 1999, *A&A*, 344, 897
- Fabrycky D. & Tremaine S., 2007, *ApJ*, 669, 1298
- Fabrycky, D. C., Lissauer, J. J., Ragozzine, D. et al. 2014, *ApJ*, 790, 146
- Fekel, F. C., Willmarth, D. W., Abt, H. A. & Pourbaix, D. 2018, *AJ*, 156, 117
- Gaia Collaboration, Brown, A. G. A., Vallenari, A., Prusti, T. et al. 2018, *A&A*, in preparation (Vizier Catalog I/345/gaia2).
- Goldberg, D., Mazeh, T., Latham, D. W. et al. 2002, *AJ*, 124, 1132
- Fűrész, G. 2008, PhD thesis, University of Szeged, Hungary
- Guillout, P., Klutsch, A., Frasca, A., Freire Ferrero, R. et al. 2009, *A&A*, 504, 829
- Hartkopf, W.I., McAlister, H.A., Mason, B.D. et al. 1994, *AJ* 108, 2299
- Hartkopf, W. I., Mason, B. D. & Worley, C. E. 2001, *AJ*, 122, 3472
- Heasley, J. N., Franz, O. G., Wasserman, L. H., & Horch, E. P. 2002, *BAAS*, 34, 1095
- Heintz, W. D. 1969, *AJ*, 74, 768
- Heintz, W. D. 1990, *AJ*, 99, 420
- Heintz, W. D. 1993, *AJ*, 105, 1188
- Horch, E. P., Franz, O. G., Wasserman, L. H., & Heasley, J. N. 2006, *AJ*, 132, 836
- Horch, E. P., Bahi, L. A. P., Gaulin, J. R. et al. 2012, *AJ*, 143, 10
- Horch, E. P., van Altena, W. F., Demargue, P. et al. 2015a, *AJ*, 149, 151
- Horch, E. P., van Belle, G. T., Davidson, J. W., Jr. et al. 2015b, *AJ*, 150, 151
- Horch, E. P., Casetti-Dinescu, D. I., Camarata, M. A. et al. 2017, *AJ*, 153, 212
- Horch, E. I., Tokovinin, A., Weiss, S. A. et al. 2019, *AJ*, 157, 56
- Jancart, S., Jorissen, A., Babusiaux, C., & Pourbaix, D. 2005, *A&A*, 442, 365
- Janson, M., Hormuth, F., Bergfors, C., et al. 2012, *ApJ*, 754, 44
- Kostov, V. B., Orosz, J. A., Welsh, W. F. et al. 2016, *ApJ*, 827, 86
- 2016ApJ...827...86K Kepler-1647 1100 d around 11-d SB
- Latham, D. W. 1992, in *IAU Coll. 135, Complementary Approaches to Double and Multiple Star Research*, ASP Conf. Ser. 32, eds. H. A. McAlister & W. I. Hartkopf (San Francisco: ASP), 110
- Latham, D. W., Stefanik, R. P., Torres, G. et al. 2001, *AJ*, 124, 1144
- Ling, J. 2012, *IAU Inf. Circ.* 176, 1
- Mante, R. 2000, *IAU Inf. Circ.*, 140, 1
- Mason, B. D., Wycoff, G. L., Hartkopf, W. I. et al. 2001, *AJ*, 122, 3466 (WDS)
- Moe, M. & Kratter, K. M. 2018, *ApJ*, 854, 44
- Perryman, M. A. C., Lindegren, L., Kovalevsky, J. et al. 1997, *A&A*, 323L, 49 (Vizier Catalog I/239/hip\_main)
- Roberts, L. C., Jr., Tokovinin, A., Mason, B. D. et al. 2015, *AJ*, 150, 130
- Roberts, L. C., Jr. & Mason, B. D. 2018 *MNRAS*, 473, 4497
- Scardia, M., Priour, J.-L., Panseccchi, L., & Argyle, R. W. 2012, *IAU Inf. Circ.* 177, 1
- Scott, N. J., Howell, S. B., Horch, E. P., & Everett, M. E. *PASP*, 2018, 130, 054502
- Sperauskas et al. 2019, *A&A*, accepted (preprint arXiv:1904.06544)
- Szentgyorgyi, A. H., & Fűrész, G. 2007, *Precision Radial Velocities for the Kepler Era*, in *The 3rd Mexico-Korea Conference on Astrophysics: Telescopes of the Future and San Pedro Mártir*, ed. S. Kurtz, RMxAC, 28, 129
- Tokovinin, A. 2016, *ORBIT: IDL software for visual, spectroscopic, and combined orbits*. Zenodo, doi:10.2581/zenodo.61119
- Tokovinin, A. 2017, *ApJ*, 844, 103
- Tokovinin, A. 2018a, *PASP*, 130, 5002
- Tokovinin, A. 2018b, *ApJS*, 235, 6
- Tokovinin, A. 2018, *AJ*, 155, 160
- Tokovinin, A. A. & Smekhov, M. G. 2002, *A&A*, 382, 118
- Tokovinin, A., Mason, B. D., & Hartkopf, W. I. 2010, *AJ*, 139, 743
- Tokovinin, A., Latham, D. W., & Mason, B. D. 2015, *AJ*, 149, 195
- Tokovinin, A. & Latham, D. W. 2017, *ApJ*, 838, 54
- Tokovinin, A., Mason, B. D., Hartkopf, W. I., Mendez, R. A. & Horch, E. P. 2018, *AJ*, 155, 235
- Zucker, S., & Mazeh, T. 1994, *ApJ*, 420, 806
- Zucker, S., Torres, G., & Mazeh, T. 1995, *ApJ*, 452, 863